

# Passive, wireless transduction of electrochemical impedance across thin-film microfabricated coils using reflected impedance

Alex Baldwin<sup>1</sup> · Lawrence Yu<sup>1</sup> · Madelina Pratt<sup>1</sup> · Kee Scholten<sup>1</sup> · Ellis Meng<sup>1,2</sup>

© Springer Science+Business Media, LLC 2017

**Abstract** A new method of wirelessly transducing electrochemical impedance without integrated circuits or discrete electrical components was developed and characterized. The resonant frequency and impedance magnitude at resonance of a planar inductive coil is affected by the load on a secondary coil terminating in sensing electrodes exposed to solution (reflected impedance), allowing the transduction of the high-frequency electrochemical impedance between the two electrodes. Biocompatible, flexible secondary coils with sensing electrodes made from gold and Parylene C were microfabricated and the reflected impedance in response to phosphate-buffered saline solutions of varying concentrations was characterized. Both the resonant frequency and impedance at resonance were highly sensitive to changes in solution conductivity at the secondary electrodes, and the effects of vertical separation, lateral misalignment, and temperature changes were also characterized. Two applications of reflected impedance in biomedical sensors for hydrocephalus shunts and glucose sensing are discussed.

**Keywords** Electrochemical impedance · Reflected impedance · Passive · Wireless · Sensor · Coils · Inductive coupling · Glucose sensing · Hydrocephalus

✉ Ellis Meng  
ellis.meng@usc.edu

<sup>1</sup> Department of Biomedical Engineering, Viterbi School of Engineering, University of Southern California, 1042 Downey Way, DRB-140, Los Angeles, CA 90089-1111, USA

<sup>2</sup> Ming Hsieh Department of Electrical Engineering, Viterbi School of Engineering, University of Southern California, 3651 Watt Way, VHE-602, Los Angeles, CA 90089-0241, USA

## 1 Introduction

Numerous biomedical applications require measuring the electrochemical impedance between two or more electrodes. *In vivo* electrochemical impedance measurement has been used to predict heart failure (Yu et al. 2005) and monitor the effectiveness of deep brain stimulation (Scott et al. 2009), and impedance-based biosensors have been developed to monitor biomarkers (Yang et al. 2004; Elshafey et al. 2013) or physical parameters such as the flow rate (Baldwin et al. 2016a; 2016b) and pressure (Yu and Meng 2014; Yu et al. 2016) of cerebrospinal fluid or the force applied to an intracortical probe (Kim et al. 2013; Kim et al. 2015). These applications often use microfabricated electrodes which can be implanted in the human body, but measuring the electrochemical impedance between these electrodes typically requires space-consuming electronics which access the electrodes via percutaneous connections. Integrated circuits designed to measure impedance and wirelessly transmit data out of the body have been developed (Min et al. 2001; Li et al. 2005; Ahmadi and Jullien 2009), but the technology is fundamentally incompatible with the aqueous ionic environment found *in vivo* (Vanhoestenbergh and Donaldson 2013) and requires bulky hermetic packaging or encapsulation by a biocompatible polymer such as Parylene C (Stieglitz et al. 2002; Hassler et al. 2010), which is prone to water penetration and failure under chronic *in vivo* conditions. In any case, discrete and integrated electronics add cost and complexity to an implantable device. A passive method of measuring electrochemical impedance which does not require implanted integrated circuits or discrete components would allow for a wide range of simple, long-lasting implantable devices.

Passive implantable devices which pair an inductive coil with a capacitive sensor have been widely explored in literature (Bäcklund et al. 1990; Akar et al. 2001; Fonseca

et al. 2006; Chen et al. 2014). By placing the inductive coil in series with a variable capacitor whose value varies with a parameter such as fluidic pressure, a wireless sensor is realized that achieves transduction by monitoring the implanted coil's resonance. If the inductive coil's quality factor is high enough, a phase dip representing the secondary resonance can be detected via either radiofrequency or inductive coupling. This principle has been used commercially to develop a passive implantable sensor for detecting atrial pressure (Abraham et al. 2011), and has been explored for implantable sensors for intraocular pressure (Katuri et al. 2008; Chen et al. 2010; Xue et al. 2012), among other applications. However, this method cannot be used to transduce the high-frequency electrochemical impedance across electrodes, as this impedance is primarily resistive and is dominated by the solution resistance between the electrodes. Furthermore, passive wireless transduction of capacitance requires an implanted coil with a high quality factor, so that its resonance peak is detectable outside the body, and a large, high-powered external coil. Even with a low-resistance secondary coil, the high resistive component of the load reduces the quality factor by several orders of magnitude.

Here, we present a novel method for passive wireless transduction of high-frequency electrochemical impedance. The resonance of an external primary coil can be altered through inductive coupling by an implanted, microfabricated secondary coil in series with a sensor responding to local changes. By placing sensor electrodes on the terminals of the secondary coil, the primary resonance can be used to wirelessly transduce the electrochemical impedance between those electrodes. Since the primary coil is outside the body, the primary resonance peak can be directly measured, allowing highly sensitive measurement and avoiding many issues experienced in other reported sensors which rely on a weak resonance signal transmitted from the implanted secondary coil. The reflected impedance at the primary resonant frequency will change based on the electrochemical impedance between the secondary electrodes, and if the secondary coil's resonant frequency is close to, but not identical to, the primary coil's resonant frequency, the primary resonant frequency will shift toward the secondary resonant frequency to a degree determined by the electrochemical impedance between the secondary electrodes, enabling a second parallel method of reflected impedance transduction. A high quality factor is not required for accurate and sensitive electrochemical impedance transduction using these methods, and we achieved transduction using secondary coils with a quality factor  $< 0.1$ . Here, we present the theory behind reflected impedance and the construction and characterization of passive, biocompatible, thin-film devices which can transduce electrochemical impedance over a wide range of solution resistances, as well as two potential biomedical applications of the method.

## 2 Theory

When a system of conductive coils is stimulated with a time-varying electric field, a coupled magnetic field is induced which can be used for energy transfer. Inductive energy transfer is commonly used in transformers, which transfer energy with minimal attenuation through a common ferrite core (Horowitz et al. 1980). More recently, energy transfer between planar coils separated by an air gap has become common for charging smartphones and other consumer electronics, though significant attenuation can occur and coils must be parallel and separated by a distance less than their radius (Hui 2013). The magnitude of inductive energy transfer between planar coils depends on the geometry of the coils, their orientation relative to each other, the frequency at which energy is transferred, and the load on the secondary side. For most applications, the resonant frequencies of the primary and secondary planar coils are matched and the two coils are positioned in parallel and concentrically.

A system of two coupled coils can be modeled as a pair of RLC circuits with mutual induction between the two coil inductances. For an ideal case with no trace resistance on the coil, the only loss in the system is through the load on the secondary coil. If the coil terminates in a pair of electrodes exposed to solution, then at high frequencies, the load will consist of the solution resistance between the electrodes and the amount of energy absorbed by the secondary coil will vary with changes in solution resistance. Since the primary and secondary coils are inductively coupled, changes in the energy absorbed by the secondary coil can be transduced by measuring the impedance reflected on to the primary coil.

We used reflected impedance to wirelessly transduce the solution resistance between a pair of electrodes in series with the secondary coil (Fig. 1). The circuit model for this system consists of a primary side parallel RLC circuit with a resistance in series with the inductance to

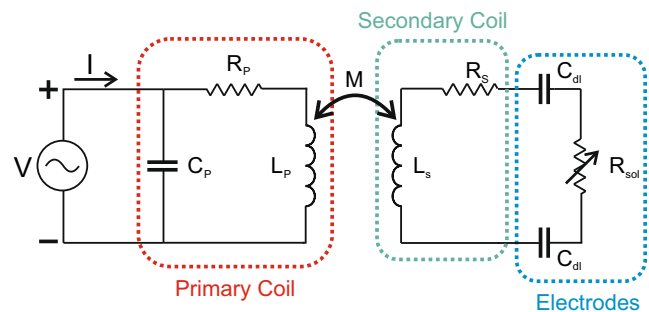


**Fig. 1** The circuit model for the wireless sensing system: a primary coil is magnetically coupled to a secondary coil which terminates in a pair of sensor electrodes. On the primary side (left),  $L_p$  is the primary coil inductance,  $C_p$  is the parallel capacitance between windings, and  $R_p$  is primary coil winding resistance. On the secondary side (right),  $L_s$  is the secondary coil inductance,  $R_s$  is the trace resistance of the secondary coil windings,  $C_{dl}$  is the double layer capacitance of each electrode, and  $R_{sol}$  is the solution resistance between electrodes.  $M$  represents the mutual inductance between primary and secondary coils.

model the winding resistance of the coil. The inductance is mutually coupled with a secondary circuit consisting of a secondary coil inductance and winding resistance and a simplified Randles circuit (Randles 1947) for the electrodes and solution; the Randles circuit includes the double layer capacitance of each electrode and the solution resistance between them. This circuit can be linearized as shown in Fig. 2, where the primary and secondary coils are coupled by a mutual inductor of value  $M = k\sqrt{L_P L_S}$ , where  $k$  is a coupling coefficient which varies from 0 to 1 based on coil geometry and orientation, and the leakage inductance due to incomplete coupling is represented as inductors of value  $L_P - M$  and  $L_S - M$ . The impedance of this circuit as seen from the primary coil can be written as

$$Z = \frac{(L_P/C_P + R_P/j\omega C_P)Z_S - j\frac{\omega M^2}{C_P}}{\left(1/j\omega C_P + j\omega L_P + R_P\right)Z_S + \omega^2 M^2} \tag{1}$$

$$Z_S = j\omega L_S + R_S + 2/j\omega C_{dl} + R_{sol}$$

To explore the effects of the secondary coil’s reflected impedance on the primary-side impedance, the primary winding resistance can be assumed to be negligible ( $R_P = 0$ ) and the impedance  $Z$  can be evaluated at the primary coil’s natural frequency  $\omega = 1/\sqrt{L_P C_P}$ . Under these conditions the impedance is

$$Z = \frac{L_P^2 Z_S - j\frac{M^2 L_P}{\sqrt{L_P C_P}}}{M^2} \tag{2}$$

Thus, the magnitude of impedance at the primary resonant frequency is related to the secondary coil’s impedance ( $Z_S$ ). As the coupling between the coils goes to zero ( $M = 0$ ) the impedance would become infinite. It is also clear that with the introduction of a secondary coil, the resonant frequency of the system is no longer equal to the resonant frequency of the primary coil alone, since there is an imaginary component inherent to the secondary impedance.

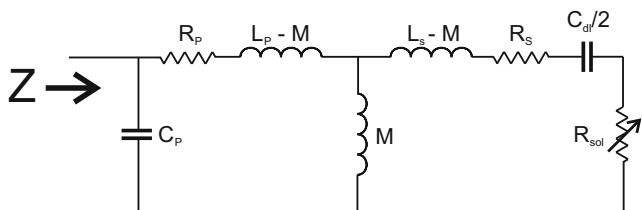


**Fig. 2** The linearized circuit model of Fig. 1, showing the leakage inductances ( $L_P - M$  and  $L_S - M$ ).  $Z$  represents the complex impedance of the circuit as seen from the primary coil terminals

Equation (2) can be expanded under the condition of non-zero  $R_P$ , and under the assumption that the natural frequencies of the primary and secondary coils are equal, i.e.  $\omega = 1/\sqrt{L_P C_P} = \sqrt{2/L_S C_{dl}}$ .

$$Z = \frac{L_P^2(R_S + R_{Sol}) - j\left(\frac{L_P M^2}{\sqrt{L_P C_P}} + (R_S + R_{Sol})R_P L_P \sqrt{L_P C_P}\right)}{M^2 + R_P L_P C_P (R_S + R_{Sol})} \tag{3}$$

This expression reveals that both the real and imaginary components of the system’s impedance are dependent on the load of the secondary coil, which for our system consists of the secondary coil resistance ( $R_S$ ) and the solution resistance ( $R_{sol}$ ). This suggests that the resonant frequency, where the imaginary component of impedance is zero, can be used to transduce the secondary load. By measuring impedance over a range of frequencies near the expected resonant frequency of the primary coil, the resonant frequency of the system and the magnitude of the impedance at resonance can both be identified, and either of these values can be used to transduce solution resistance.

The effect of changing the solution resistance on both the resonant frequency and the impedance of the system at resonance was evaluated using MATLAB. A Simulink model of the equivalent circuit in Fig. 2 was developed, and the resonant frequency and impedance magnitude at resonance were evaluated over a range of solution resistances, shown in Fig. 3. Simulations were also run which evaluated the relationship between solution resistance and both impedance magnitude and resonant frequency over a range of coupling coefficients, secondary inductances, and secondary capacitances. These simulations elucidated a direct relationship between both the resonant frequency and impedance at resonance of the system and the solution resistance across the electrodes. The sensitivity of this relationship increases with the coupling between the two coils. The relationship between impedance at resonance and solution resistance is most sensitive when the resonant frequencies (with load) of the primary and secondary coils are equal. More interestingly, the relationship between resonant frequency and solution resistance displays an inflection point where the primary and secondary resonance is lower than the primary, a lower solution resistance will cause the system’s resonant frequency to drop, and when the secondary resonance is higher the full system’s resonant frequency will rise. The secondary coil can be imagined as “pulling” the system’s resonant frequency toward itself with a strength inversely proportional to the secondary load.

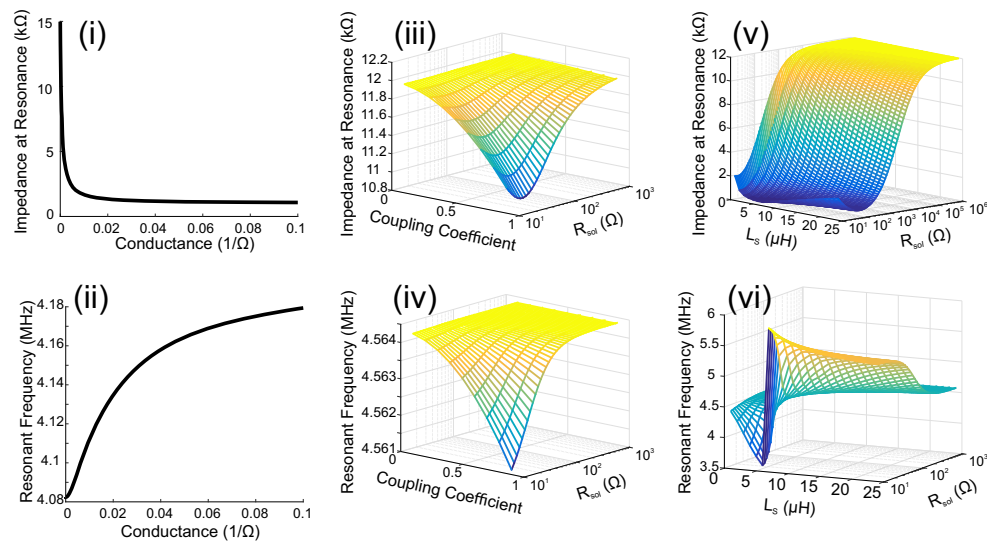


**Fig. 3** Results of simulating the effects of changing solution resistance on the reflected impedance as seen from the primary coil. The **(i)** impedance at resonance and **(ii)** resonant frequency were both found to change with solution resistance under order-of-magnitude estimates of circuit element values ( $R_p = 1 \Omega$ ,  $L_p = 30 \mu\text{H}$ ,  $C_p = 2 \text{ nF}$ ,  $L_s = 20 \mu\text{H}$ ,  $R_s = 100 \Omega$ ,  $C_{dl} = 5 \text{ nF}$ ,  $k = 0.4$ ). In another simulation, increasing the coupling coefficient  $k$  was found to increase the sensitivity of both **(iii)**

impedance magnitude and **(iv)** resonant frequency to changes in solution resistance ( $R_p = 1 \Omega$ ,  $L_p = 24 \mu\text{H}$ ,  $C_p = 2 \text{ nF}$ ,  $L_s = 4 \mu\text{H}$ ,  $R_s = 1 \Omega$ ,  $C_{dl} = 5 \text{ nF}$ ), and by varying the secondary inductance  $L_s$  it was found that **(v)** the sensitivity of impedance magnitude is maximized and **(vi)** the sensitivity of resonant frequency has an inflection point where the primary and secondary resonant frequencies are the same

### 3 Experimental methods

#### 3.1 Test coil fabrication

To explore the use of reflected impedance for wireless *in vivo* sensing, test coils were designed and fabricated (Figs. 4 and 5). Coils were fabricated from gold film on a thin substrate of Parylene C, a biocompatible and flexible thin film polymer widely used in implantable medical devices. Each coil had an outer diameter of 30 mm and consisted of 100  $\mu\text{m}$  wide and 200 nm thick gold traces which terminated in square electrodes with an exposed area of  $300 \times 300 \mu\text{m}^2$ . Three different types of coils were fabricated, with 1, 5, or 16 turns each.

Fabrication followed standard processes for Parylene-based MEMS devices (Kim and Meng 2015). First, 10  $\mu\text{m}$  of Parylene C was chemical vapor deposited onto a silicon carrier wafer. 200 nm Au, with a 20 nm Ti adhesion layer, was electron-beam deposited onto the Parylene and patterned via liftoff using a 2  $\mu\text{m}$  layer of AZ 5214 image reversal

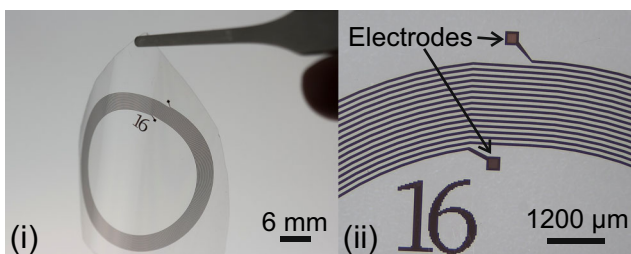


**Fig. 4** **(i)** Thin-film gold coils were fabricated on a flexible Parylene C substrate. **(ii)** Each coil terminated in two exposed electrodes of area  $300 \times 300 \mu\text{m}^2$

photoresist (EMD Performance Materials). A second 10  $\mu\text{m}$  layer of Parylene C was deposited, and electrode pads were exposed using reactive ion etching with oxygen plasma, with 15  $\mu\text{m}$  of AZ 4620 photoresist (EMD Performance Materials) used as an etch mask. Finally, devices were cut out of the wafer by hand and released by gently peeling while the wafer was immersed in deionized water.

#### 3.2 Testing and characterization

The thin-film coils were first characterized and then their effectiveness for transducing solution resistance via the reflected impedance method determined. First, 1, 5, and 16 turn coils were directly characterized by measuring DC resistance, and the inductance and quality factor at the expected measurement frequency of 5 MHz. Next, the effects of changing solution resistance on the coil's reflected impedance was characterized using phosphate-buffered saline (PBS) solutions of concentration 0.5 $\times$ , 1 $\times$ , 5 $\times$ , and 10 $\times$ , with >18  $\text{M}\Omega\cdot\text{cm}$  deionized (DI) water used as a control. Further characterization was performed on 16-turn coils using 1 $\times$  PBS to evaluate the effects

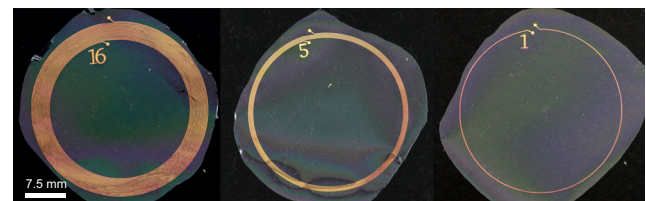


**Fig. 5** Three variations of the secondary coil, with 1, 5, or 16 turns each, were fabricated and tested. All coils had an outer radius of 30 mm

of vertical separation, lateral offset, and changes in solution temperature on reflected impedance. Vertical separation was achieved by stacking 1 mm thick glass slides between the primary and secondary coils.

DC resistance was measured using a digital multimeter and inductance and quality factor were measured using an HP 4285A precision LCR meter (75 kHz–30 MHz, 1 V<sub>pp</sub>). For reflected impedance measurement, the precision LCR meter was attached to a ferrite-cored planar coil from Wurth Electronics (24  $\mu$ H, Q = 180 @ 125 kHz, 50 mm diameter, 22 turns), which served as a primary coil, and a custom LabVIEW program was used to sweep the measurement frequency while measuring complex impedance. The microfabricated secondary coils were held in a petri dish with a 1 mm thick base which was positioned directly on top of the primary coil (Fig. 6). For each measurement, 100  $\mu$ L of PBS or DI water was placed on the electrodes using a calibrated syringe and impedance was measured using the LCR meter. The coil was triple-rinsed with DI water and re-centered between each individual measurement. PBS concentrations of 0.5 $\times$ , 1 $\times$ , 5 $\times$ , and 10 $\times$  correspond to solution conductivities of 8, 16, 80, and 160 mS/cm respectively and 1 $\times$  PBS is a common analog for physiological fluids and is isotonic with cerebrospinal fluid.

For each measurement, the complex impedance was measured over a range of frequencies around the expected primary resonant frequency, with a frequency resolution of 1 kHz. Both the resonant frequency and the magnitude of impedance at resonance were evaluated as possible impedance transduction methods. The resonant frequency was defined as the frequency at which the system's response is fully real, i.e. the phase is zero, and the impedance at resonance is the magnitude of impedance at the resonant frequency.

## 4 Results

The DC resistance, quality factor, and inductance values for the 1, 5 and 16 turn secondary coils are presented in Table 1. At high frequencies, the skin effect can cause a significant increase in the resistance of a wire or trace (Wheeler 1942), but as the thickness (200 nm) of the traces used here were

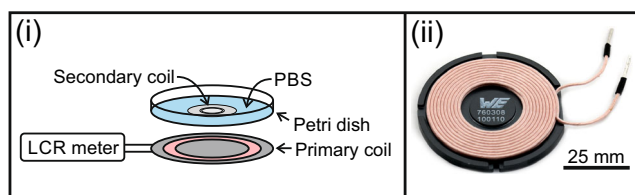


**Fig. 6** (i) Microfabricated coils were placed in a petri dish with varying concentrations of PBS and centered over a commercial primary coil connected to an LCR meter (ii) A 22-turn primary coil with a rated resonant frequency of 5 MHz (Wurth Electronics, 24  $\mu$ H, Q = 180 @ 125 kHz, 50 mm diameter)

**Table 1** The DC resistance, and the inductance and quality factor at 5 MHz, of 1, 5, and 16 turn microfabricated thin-film coils

Turns	DC Resistance	Inductance	Q
1	136.4 $\Omega$	0.121 $\mu$ H	0.05
5	605.9 $\Omega$	1.625 $\mu$ H	0.08
16	3890 $\Omega$	35.9 $\mu$ H	0.33

much thinner than the skin depth in gold at the MHz frequencies of interest ( $\sim 10$ 's of  $\mu$ m), the skin effect was negligible.

To identify the resonant frequency of the coupled system, the system's impedance was measured on the primary from 3 to 10 MHz, with DI water used to complete the circuit on the secondary coil. A peak in system impedance and an inflection point in phase was seen around 5.4 MHz, which corresponds to the expected resonant frequency of the primary coil (Fig. 7).

A significant drop in the system impedance at resonance with increasing conductivity was observed for all three coils; the 16 turn secondary coil showed the largest sensitivity. Despite rinsing and re-centering coils by hand between measurements, the measurement error was minimal; the average standard deviation of a measurement was 13.0  $\Omega$  (Fig. 8).

The resonant frequency was also sensitive to solution resistance changes, though for the 1-turn coil, the effect was not significant and for the 5-turn coil the effect was very small. When testing the 16-turn coil, however, the resonant frequency significantly increased with an increase in conductivity. The average standard deviation of a measurement was 659 Hz (Fig. 9).

Due to the high sensitivity of the 16-turn coil, this coil was used to assess the effects of primary to secondary vertical separation and misalignment. When 1 $\times$  PBS was applied to the secondary coil, the system impedance at resonance increased in a somewhat linear manner as the coils were separated, while the resonant frequency was found to drop between 1 mm and 2 mm of separation but was not observed to change significantly for greater distances (Fig. 10-i). However, when the impedance at resonance and resonant frequency were tested across the full range of PBS concentrations, the sensitivity of resonant frequency to secondary electrode impedance was seen to decrease with increasing separation between the primary and secondary coils (Fig. 10-ii, iii).

Misalignment tests also showed a change in response for both the impedance at resonance and the resonant frequency (Fig. 11). Both the resonant frequency and the impedance at resonance increased during misalignment, leveling off at around 15 mm displacement, at the radius of the secondary coil.

Additional tests were performed on a 16-turn test coil to evaluate the response of reflected impedance to changes in solution temperature. The solution resistance of an aqueous ionic solution is proportional to temperature, and changes in temperature can be measured via the electrochemical

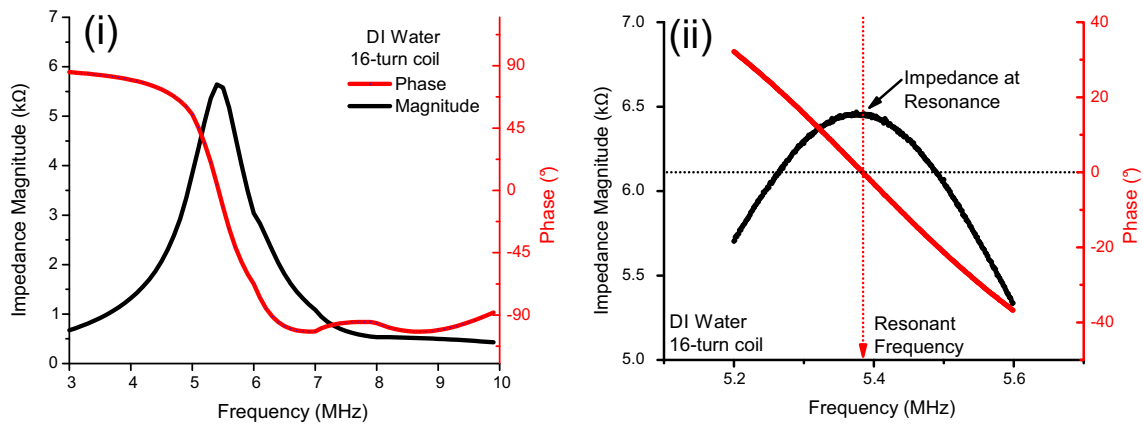


**Fig. 7** (i) The impedance of the primary coil – secondary coil system between 3 and 10 MHz shows a clear resonance peak close to 5.4 MHz. (ii) Both the resonant frequency and the impedance magnitude at

resonance were used to transduce solution resistance across the measurement electrodes on the secondary

impedance between two electrodes (Baldwin et al. 2016a). When measuring reflected impedance, the impedance magnitude at resonance decreased and the resonant frequency increased with increasing temperature, which is consistent with the decrease in solution resistance expected (Fig. 12).

### 5 Applications

In addition to characterization and measurement of the conductivity of PBS using microfabricated test coils, applications which could use reflected impedance for *in vivo* sensing were explored. Two applications in particular showed promising preliminary results: catheter patency sensing for hydrocephalus shunts, and wireless glucose sensing.

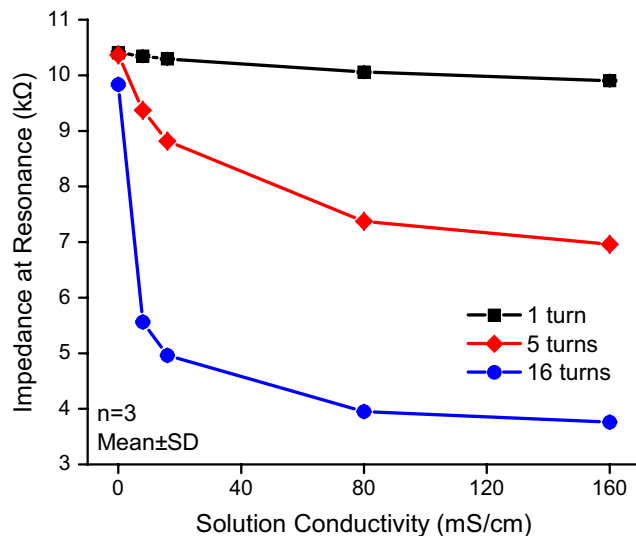


**Fig. 8** The system impedance magnitude at resonance was related to the conductivity of solution across the electrodes, which is inversely proportional to measured impedance at the sensing electrodes. Error bars are present but not visible in most cases; the average standard deviation was 13.0 Ω

### 5.1 Catheter patency sensing

Protein and debris buildup in implanted catheters can cause progressive occlusion and failure. This phenomenon has been reported for central venous catheters (Mirza et al. 2004; Shah and Shah 2008), hemodialysis catheters (Palder et al. 1985), and insulin pumps (van Bon et al. 2012), and is common in hydrocephalus shunts, which drain excess cerebrospinal fluid from the brain’s ventricles to the abdomen (Aschoff et al. 1999; Drake et al. 2000; Tuli et al. 2000). We previously reported a patency sensor which directly transduces partial catheter occlusion using the electrochemical impedance through a ventricular catheter, allowing doctors to monitor progressive blockage and predict hydrocephalus shunt failure (Kim et al. 2016). Here we use reflected impedance to develop a wireless patency sensor which can transduce progressive

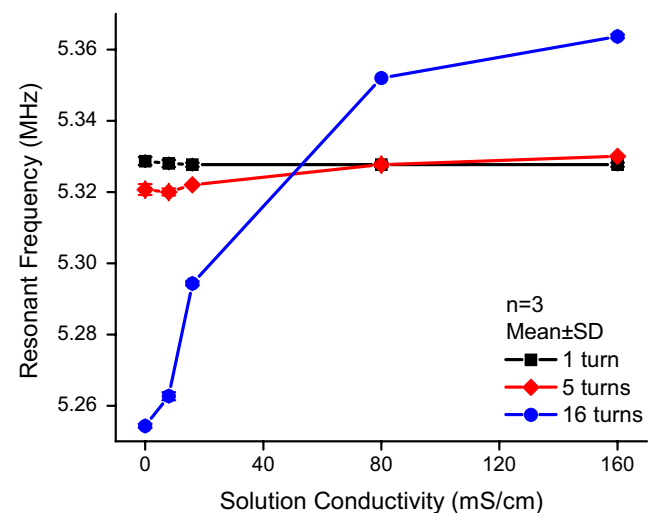


**Fig. 9** The resonant frequency was also related to conductivity across the electrodes of the 16-turn and 5-turn devices, but the effect was only substantial for the 16-turn device. Error bars are present; the average standard deviation was 659 Hz

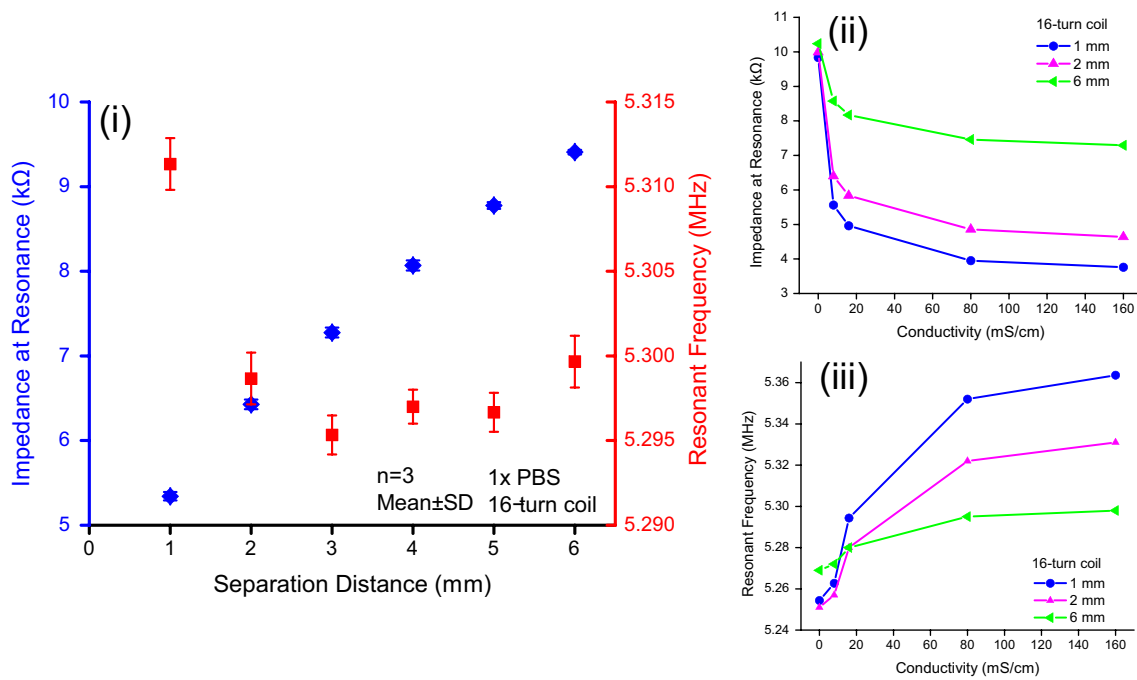


**Fig. 10** Reflected impedance of a 16-turn secondary coil was measured as the secondary coil was separated vertically from the primary coil using 1 mm thick glass slides. **(i)** When 1× PBS was applied to the secondary coil, the impedance at resonance increased linearly as the coils were

separated, while the resonant frequency saw a slight decrease and then relative stability. However, the sensitivity of both **(ii)** the impedance at resonance and **(iii)** the resonant frequency to changes in solution conductivity decreased when separated from the primary coil

blockage without the use of integrated circuits or discrete electronic components.

To simulate proximal catheters with varying degrees of occlusion, silicone tubes 1 mm in diameter were sealed at one end and bored with holes 500 μm in diameter, matching commercial proximal catheters. These tubes were placed in a beaker containing 100 mL of 1× PBS and filled. Instead of a thin-film microfabricated coil, a secondary coil was made using a 3D printed module designed to fit in line with currently-used hydrocephalus shunts. 34 AWG copper wire was wrapped around a slit in its center, creating a 12-turn secondary coil ( $L = 4.31 \mu\text{H}$  @ 1 MHz,  $Q = 23.4$ ,  $R_{DC} = 1.2 \Omega$ ) (Fig. 13-i).

Each end of the coil was connected to a platinum electrode, with one electrode inserted into the silicone catheters above the holes and one electrode placed in the beaker of PBS. This secondary coil was centered above the primary coil and reflected impedance was measured non-consecutively through catheters with 12, 8, 4, 2, and 0 open holes (Fig. 13-ii).

The impedance through these catheters ranged from 26.5 kΩ for a catheter with 12 open holes to 31.5 kΩ for a catheter with 2 open holes, which according to simulations is outside the region of maximum sensitivity for reflected impedance. Despite this, progressive blockage could be clearly transduced by measuring the impedance

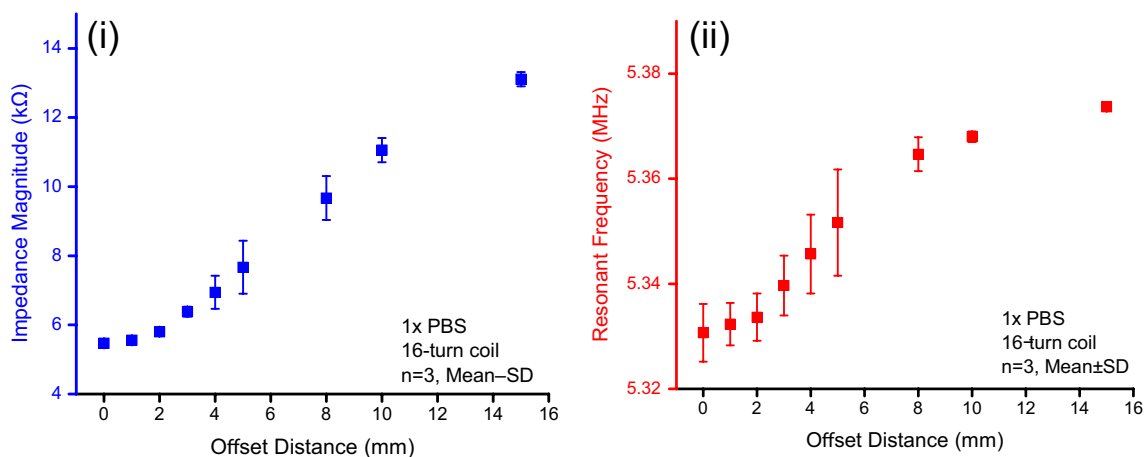


**Fig. 11** When the coil was offset from center, both the **(i)** impedance magnitude and the **(ii)** resonant frequency increased. This increase began to level off once the secondary coil was offset 15 mm, which is equal to its radius

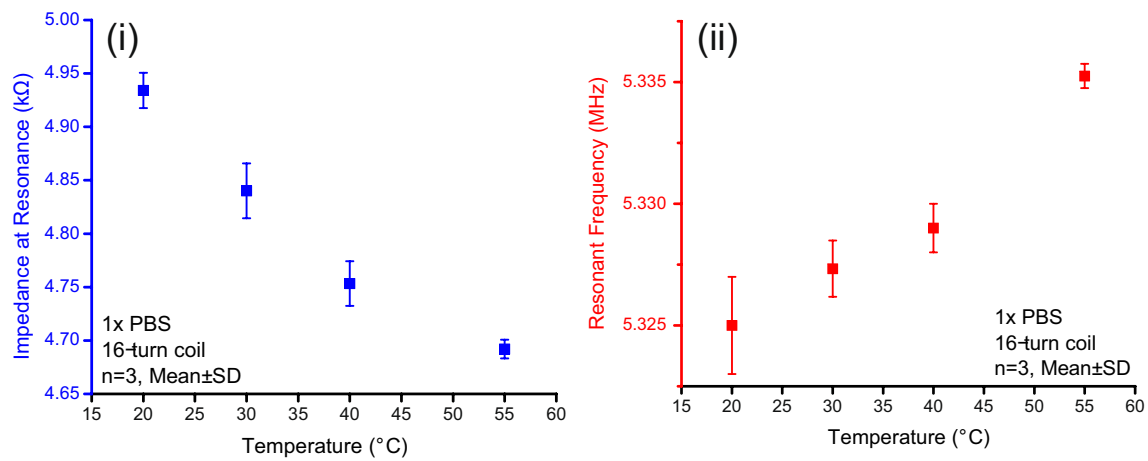


**Fig. 12** The (i) impedance magnitude at resonance decreased and the (ii) resonant frequency increased when the solution temperature increased, which is consistent with a decrease in solution resistance due to changes in ionic mobility when an ionic solution is heated

magnitude at resonance (Fig. 14). There was no significant change in the resonant frequency between catheters with different numbers of holes.

## 5.2 Glucose sensing

Glucose sensing is an important application essential for managing diabetes. The most common method of sensing glucose is to functionalize a system of electrodes by adhering glucose oxidase (GOx) to the surface (Wang 2001). When exposed to GOx, glucose is converted into gluconic acid and hydrogen peroxide, which is normally detected as a change in DC current using a 3-electrode system. Commercial glucose sensors using this principle require either the patient to prick their finger every time a measurement is made or require percutaneous leads connecting implanted electrodes to external electronics (Oliver et al. 2009). We hypothesized that the buildup of hydrogen peroxide due to the glucose-GOx reaction could be measured using high-frequency impedance, and we tested using reflected impedance to transduce glucose levels wirelessly, without additional electronics.

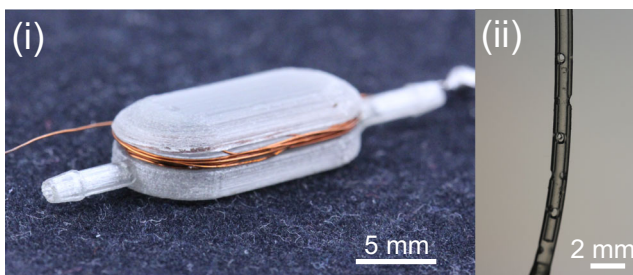


**Fig. 13** (i) A secondary coil for measuring catheter patency in hydrocephalus shunts, made by wrapping 34 AWG copper wire around a 3D-printed module compatible with current shunt technology.  $L = 4.31 \mu\text{H}$ ,  $Q = 23.4$  @ 1 MHz,  $R_{\text{DC}} = 1.2 \Omega$ . (ii) A mock proximal catheter, consisting of a silicone tube 1 mm wide with 12 open holes of 500  $\mu\text{m}$  diameter each

In a sensor which uses GOx, electrodes are typically large and as close together as possible in order to minimize baseline impedance and maximize the area available for the glucose reaction. The 16-turn coils characterized previously have electrodes spaced far apart and relatively small electrode areas, limiting their potential sensitivity. However, a preliminary attempt was made to functionalize these coils. The electrode coating process followed previously reported methods for adhering GOx to electrodes with a polymer substrate (Yu et al. 2003; Yao et al. 2011). 100  $\mu\text{L}$  of a solution of 10 mg glucose oxidase type VII per mL of 0.1x PBS was placed on the 16-turn coil's electrodes, and the coil was suspended in a sealed container above titanium isopropoxide at 30 °C for 6 h to form a sol-gel. The device was gently rinsed with DI water after coating, and 5% Nafion was added to the surface to increase sensitivity (Yao et al. 2011). The device was stored in 1x PBS at 2 °C.

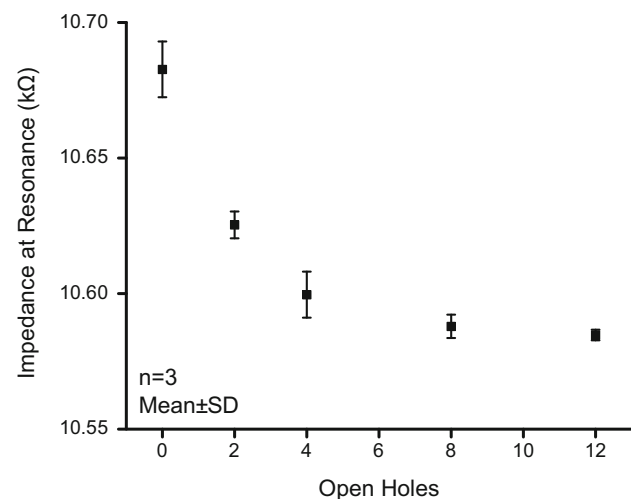


**Fig. 14** The impedance at resonance increased with decreasing number of holes, indicating that reflected impedance could be used to predict proximal catheter occlusion

During testing, the resonant frequency of the primary coil alone was found and subsequent measurements were taken at this frequency. 100  $\mu\text{L}$  of either 100 mM D-glucose dissolved in 1 $\times$  PBS or 1 $\times$  PBS without glucose were alternately placed on the electrodes, with the device rinsed with DI water between measurements. Impedance magnitude and phase was measured after 30 s of settling.

The device was tested for four days after electrode coating. There was a large difference in the baseline impedance between the four days, but a change in the reflected impedance signal was observed on each day. Figure 15 shows the difference in impedance and phase when the electrodes were exposed to PBS containing glucose versus plain PBS on the fourth day after coating. The impedance increased with the addition of glucose, and a small drop in phase was observed. These results indicate that reflected impedance may be useful for wirelessly measuring the presence of biomarkers, and future work will involve developing reflected impedance devices with larger interdigitated electrodes and optimizing the glucose oxidase coating process.

## 6 Discussion

Despite their low quality factor, 1, 5, and 16 turn thin-film coils were able to accurately transduce a wide range of solution resistances using the reflected impedance method. For all coils, the system impedance magnitude at the primary resonant frequency varied with solution resistance, and for the 16-turn coil an additional transduction method using the resonant frequency value was developed. The variance of impedance magnitude at resonance clearly matched up with theoretical and simulation results, and the large variance in primary resonant frequency seen when testing the 16-turn coil suggests that the resonant frequency of this coil, which is determined by the coil's inductance

and the double layer capacitance of the two electrodes, was slightly higher than the primary coil's resonant frequency.

Further testing using the 16-turn coil showed that accurate transduction using this reflected impedance method requires close vertical proximity and precise lateral alignment. As the secondary coil was separated vertically from the primary coil, the sensitivity of the system to changes in solution resistance decreased linearly, following the decrease in the coupling constant. Lateral misalignment also decreased coupling, and once the secondary coil's center was one secondary radius (15 mm) away from the primary coil's center, the signal stabilized, indicating that by this point the two coils were uncoupled. This shift in signal with misalignment means that close proximity and confidence in primary coil alignment are required for any practical application of this technique, which for an implantable sensor means that the secondary coil must be placed just under the skin. The shift in resonant frequency with vertical misalignment presents a major disadvantage over passive capacitive sensors, which measure the resonance of a high-Q secondary coil directly and only experience a decrease in their sensor's signal to noise ratio when their primary coil is vertically separated from their sensor.

Despite its limitation, this method presents a number of advantages over currently-used implantable sensors. No other sensing method has been developed which can wirelessly transduce a resistive load without the use of discrete electrical components or integrated circuits. Our method does not require a high secondary quality factor and in fact showed remarkable accuracy and sensitivity using coils with  $Q < 0.5$ , which allows for thin-film, fully flexible sensors and removes the need for the complex fabrication steps and thick, electroplated metal layers used in previously reported thin-film coils. The two parallel methods of transduction available from a single coil allow for redundancy and the detection of certain failure modes.

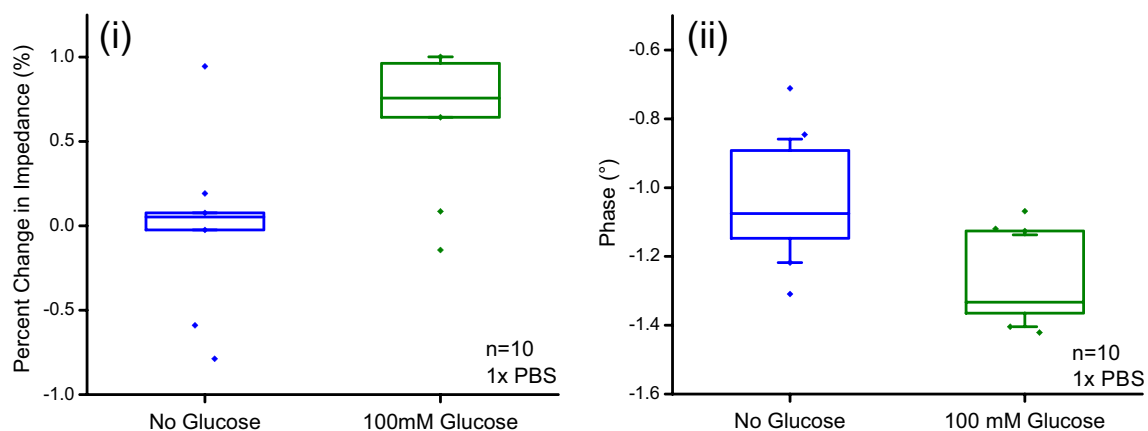


**Fig. 15** A 16-turn coil coated with a GOx/titanium isopropoxide sol-gel was alternately exposed to PBS with and without 100 mM d-glucose. When impedance was measured at the primary coil's resonant frequency,

(i) the impedance magnitude increased and (ii) the phase slightly decreased on exposure to the glucose-containing solution. This effect was still present up to 4 days after coating (data shown)

The optimal applications for reflected impedance, therefore, are implantable sensors which sit near the surface of the skin and transduce loads based on high-frequency impedance or resistance. Two applications were explored which met these requirements: catheter patency sensing in hydrocephalus shunts, and glucose sensing. The valves of hydrocephalus shunts typically sit just under the skin above the skull, and a method has been previously demonstrated to transduce catheter patency using high-frequency electrochemical impedance, making this application ideal for reflected impedance. A module designed to sit in-line with existing shunts was developed and progressive detection of catheter blockage using reflected impedance was demonstrated, though the sensitivity was lower than expected due to the high impedance magnitude through the catheter. Future improvements could include increasing inductance by increasing turns or adding a ferrite core and tuning the secondary electrode sizes such that the secondary resonant frequency lies in the range necessary to allow both methods of reflected impedance-based transduction. Glucose measurement is a daily routine for millions of diabetes patients worldwide and require measuring the low-frequency impedance across coated electrodes just under the skin's surface. A 16-turn coil coated in glucose oxidase showed a small but significant change in reflected impedance when exposed to glucose-containing saline, and future work will explore reflected impedance coils with large, interdigitated electrodes and more effective coating methods to enable transduction of physiologically-relevant glucose levels. Further applications for reflected impedance sensors could include passive dose sensing in implanted micropumps. Dose sensing based on high-frequency electrochemical impedance has already been demonstrated in an electrolysis-based implantable micropump (Gutierrez et al. 2011; Sheybani et al. 2015), and applications such as passive drug delivery to ocular tissue (Lo et al. 2009) could also benefit from a flexible, passive, thin-film dose sensor.

## 7 Conclusion

A new method for passive, wireless sensing of high-frequency electrochemical impedance based on the reflected impedance across inductively coupled coils was developed and characterized. Tests performed using microfabricated thin-film coils showed that this method can transduce a wide range of impedance values by monitoring either the primary resonant frequency or the impedance at resonance, with extremely high sensitivities achieved for both methods despite very low quality factors on the secondary coils. Several disadvantages do exist with reflected impedance, namely that vertical or lateral misalignment will cause progressive coil decoupling and will interfere with signal transduction, but to the best of our knowledge this method is the only reported method of passively

measuring resistive loads without integrated circuits or discrete electronic components. This method lends itself well to the development of wireless impedance-based sensors for implantation in the human body; two potential applications in hydrocephalus treatment and glucose sensing were explored, and future work will continue to apply and optimize reflected impedance for the development of biomedical sensors.

**Acknowledgements** The authors would like to thank Ewina Pun and Sam Huynh for their help with device characterization, Dr. Donghai Zhu of the Keck Photonics Lab for assistance with fabrication, and all the members of the Biomedical Microsystems Lab of USC for their advice and support. This work was supported in part by the National Science Foundation under award EFRI-1332394.

## References

- W.T. Abraham, P.B. Adamson, R.C. Bourge, M.F. Aaron, M.R. Costanzo, L.W. Stevenson, W. Strickland, S. Neelagaru, N. Raval, S. Krueger, Wireless pulmonary artery haemodynamic monitoring in chronic heart failure: A randomised controlled trial. *Lancet* **377**(9766), 658–666 (2011)
- M.M. Ahmadi, G.A. Jullien, A wireless-implantable microsystem for continuous blood glucose monitoring. *IEEE Trans. Biomed. Circuits Syst.* **3**(3), 169–180 (2009)
- O. Akar, T. Akin, K. Najafi, A wireless batch sealed absolute capacitive pressure sensor. *Sensors Actuators A Phys.* **95**(1), 29–38 (2001)
- A. Aschoff, P. Kremer, B. Hashemi, S. Kunze, The scientific history of hydrocephalus and its treatment. *Neurosurg. Rev.* **22**(2–3), 67–93 (1999)
- Y. Bäcklund, L. Rosengren, B. Hök, B. Svedbergh, Passive silicon transducer intended for biomedical, remote pressure monitoring. *Sensors Actuators A Phys.* **21**(1), 58–61 (1990)
- A. Baldwin, L. Yu and E. Meng, An electrochemical-based thermal flow sensor. *Micro Electro Mechanical Systems (MEMS), 2016 I.E. 29th International Conference on, IEEE, (2016a)*
- A. Baldwin, L. Yu, E. Meng, An electrochemical impedance-based thermal flow sensor for physiological fluids. *J. Microelectromech. Syst.* **25**(6), 1015–1024 (2016b)
- P.-J. Chen, S. Saati, R. Varma, M.S. Humayun, Y.-C. Tai, Wireless intra-ocular pressure sensing using microfabricated minimally invasive flexible-coiled LC sensor implant. *J. Microelectromech. Syst.* **19**(4), 721–734 (2010)
- L.Y. Chen, B.C.-K. Tee, A.L. Chortos, G. Schwartz, V. Tse, D.J. Lipomi, H.-S.P. Wong, M.V. McConnell, Z. Bao, Continuous wireless pressure monitoring and mapping with ultra-small passive sensors for health monitoring and critical care. *Nat. Commun.* **5**, 5028 (2014)
- J. Drake, J. Kestle, S. Tuli, CSF shunts 50 years on—past, present and future. *Childs Nerv. Syst.* **16**(10–11), 800–804 (2000)
- R. Elshafey, A.C. Tavares, M. Sijaj, M. Zourab, Electrochemical impedance immunosensor based on gold nanoparticles–protein G for the detection of cancer marker epidermal growth factor receptor in human plasma and brain tissue. *Biosens. Bioelectron.* **50**, 143–149 (2013)
- M.A. Fonseca, M.G. Allen, J. Kroh, J. White, Flexible wireless passive pressure sensors for biomedical applications. *Tech. Dig. Solid-State Sensor, Actuator, and Microsystems Workshop (Hilton Head 2006), 2006*
- C.A. Gutierrez, R. Sheybani, E. Meng, Electrochemically-based dose measurement for closed-loop drug delivery applications. *Solid-*

- State Sensors, Actuators and Microsystems Conference (TRANSDUCERS), 2011 16th International, IEEE, 2011
- C. Hassler, R.P. von Metzen, P. Ruther, T. Stieglitz, Characterization of parylene C as an encapsulation material for implanted neural prostheses. *J. Biomed. Mater. Res. B Appl. Biomater.* **93**(1), 266–274 (2010)
- P. Horowitz, W. Hill, I. Robinson, *The Art of Electronics* (Cambridge university press, Cambridge, 1980)
- S. Hui, Planar wireless charging technology for portable electronic products and qi. *Proc. IEEE* **101**(6), 1290–1301 (2013)
- K.C. Katuri, S. Asrani, M.K. Ramasubramanian, Intraocular pressure monitoring sensors. *IEEE Sensors J.* **8**(1), 12–19 (2008)
- B.J. Kim, E. Meng, Micromachining of Parylene C for bioMEMS. *Polym. Adv. Technol.* **27**(5), 564–576 (2015)
- B.J. Kim, C.A. Gutierrez, E. Meng, Parylene-based electrochemical-MEMS force sensor for studies of intracortical probe insertion mechanics. *J. Microelectromech. Syst.* **24**(5), 1534–1544 (2015)
- B.J. Kim, W. Jin, A. Baldwin, L. Yu, E. Christian, M.D. Krieger, J.G. McComb, E. Meng, Parylene MEMS patency sensor for assessment of hydrocephalus shunt obstruction. *Biomed. Microdevices* **18**(5), 87 (2016)
- B. Kim, C. Gutierrez, E. Meng, *In vitro* characterization of a probe-mounted parylene-based pressure sensor array for intracortical applications. 7th Intl. Conf. on Microtechnologies in Medicine and Biology (MMB), (2013)
- Y.-T. Li, C.-H. Chang, J.-J. Chen, 陳家進, C.-C. Wang, C.-K. Liang, 梁治國, Development of implantable wireless biomicrosystem for measuring electrode-tissue impedance. *J. Med. Biol. Eng.* **25**(3), 1–7 (2005)
- R. Lo, P.-Y. Li, S. Saati, R.N. Agrawal, M.S. Humayun, E. Meng, A passive MEMS drug delivery pump for treatment of ocular diseases. *Biomed. Microdevices* **11**(5), 959 (2009)
- M. Min, T. Parve, V. Kukk, A. Kuhlberg, An implantable analyzer of bio-impedance dynamics: mixed signal approach. IMTC 2001. Proceedings of the 18th IEEE Instrumentation and Measurement Technology Conference. Rediscovering Measurement in the Age of Informatics (Cat. No.01CH 37188), 2001
- B. Mirza, V.W. Vanek, D.T. Kupensky, Pinch-off syndrome: Case report and collective review of the literature. *Am. Surg.* **70**(7), 635–644 (2004)
- N. Oliver, C. Toumazou, A. Cass, D. Johnston, Glucose sensors: A review of current and emerging technology. *Diabet. Med.* **26**(3), 197–210 (2009)
- S.B. Palder, R.L. Kirkman, A.D. Whittemore, R.M. Hakim, J.M. Lazarus, N.L. Tilney, Vascular access for hemodialysis. Patency rates and results of revision. *Ann. Surg.* **202**(2), 235 (1985)
- J.E.B. Randles, Kinetics of rapid electrode reactions. *Discuss. Faraday Soc.* **1**, 11–19 (1947)
- F.L. Scott, M. Svjetlana, D.J. Matthew, L.V. Jerrold, C.M. Cameron, *In vivo* impedance spectroscopy of deep brain stimulation electrodes. *J. Neural Eng.* **6**(4), 046001 (2009)
- P.S. Shah, V.S. Shah, Continuous heparin infusion to prevent thrombosis and catheter occlusion in neonates with peripherally placed percutaneous central venous catheters. *Cochrane Libr* (2008)
- R. Sheybani, A. Cobo, E. Meng, Wireless programmable electrochemical drug delivery micropump with fully integrated electrochemical dosing sensors. *Biomed. Microdevices* **17**(4), 74 (2015)
- T. Stieglitz, S. Kammer, K. Koch, S. Wien, A. Robitzki, Encapsulation of flexible biomedical microimplants with parylene C. *IFESS 2002* 5, (2002)
- S. Tuli, J. Drake, J. Lawless, M. Wigg, M. Lamberti-Pasculli, Risk factors for repeated cerebrospinal shunt failures in pediatric patients with hydrocephalus. *J. Neurosurg.* **92**(1), 31–38 (2000)
- A.C. van Bon, D. Dragt, J.H. DeVries, Significant time until catheter occlusion alerts in currently marketed insulin pumps at two basal rates. *Diabetes Technol. Ther.* **14**(5), 447–448 (2012)
- A. Vanhoestenbergh, N. Donaldson, Corrosion of silicon integrated circuits and lifetime predictions in implantable electronic devices. *J. Neural Eng.* **10**(3), 031002 (2013)
- J. Wang, Glucose biosensors: 40 Years of advances and challenges. *Electroanalysis* **13**(12), 983 (2001)
- H.A. Wheeler, Formulas for the skin effect. *Proc. IRE* **30**(9), 412–424 (1942)
- N. Xue, S.-P. Chang, J.-B. Lee, A SU-8-based microfabricated implantable inductively coupled passive RF wireless intraocular pressure sensor. *J. Microelectromech. Syst.* **21**(6), 1338–1346 (2012)
- L. Yang, Y. Li, G.F. Erf, Interdigitated Array microelectrode-based electrochemical impedance Immunosensor for detection of Escherichia Coli O157:H7. *Anal. Chem.* **76**(4), 1107–1113 (2004)
- H. Yao, A.J. Shum, M. Cowan, I. Lähdesmäki, B.A. Parviz, A contact lens with embedded sensor for monitoring tear glucose level. *Biosens. Bioelectron.* **26**(7), 3290–3296 (2011)
- L. Yu, E. Meng, A microbubble pressure transducer with bubble nucleation core. *Micro Electro Mechanical Systems (MEMS), 2014 I.E. 27th International Conference on, 2014*
- J. Yu, S. Liu, H. Ju, Glucose sensor for flow injection analysis of serum glucose based on immobilization of glucose oxidase in titania sol-gel membrane. *Biosens. Bioelectron.* **19**(4), 401–409 (2003)
- Yu, C.-M., L. Wang, E. Chau, R. H.-W. Chan, S.-L. Kong, M.-O. Tang, J. Christensen, R. W. Stadler and C.-P. Lau (2005). "Intrathoracic impedance monitoring in patients with heart failure." *Correlation With Fluid Status and Feasibility of Early Warning Preceding Hospitalization* **112**(6): 841–848
- L. Yu, C.A. Gutierrez, E. Meng, An electrochemical microbubble-based MEMS pressure sensor. *J. Microelectromech. Syst.* **25**(1), 144–152 (2016)